

## Distributions of the total energy and multiplicity of gamma rays feeding the discrete yrast states in heavy-ion-induced fusion reactions

I. Y. Lee, C. Baktash, J. R. Beene, M. P. Fewell,\* M. L. Halbert, N. R. Johnson, F. K. McGowan, W. T. Milner, H. J. Kim, and R. O. Sayer  
Oak Ridge National Laboratory, Oak Ridge, Tennessee 37831

D. G. Sarantites

Washington University, St. Louis, Missouri 63130

(Received 26 September 1986)

The distribution of the total energy and multiplicity of gamma rays feeding the yrast transitions has been measured for  $^{158,159}\text{Er}$ ,  $^{130}\text{Ce}$ , and  $^{116,117}\text{Te}$ , which are produced in several heavy-ion fusion reactions. The observed shape of the distribution feeding discrete yrast states varies with the spin of the yrast transition. However, the differences are small, especially for heavier-ion induced reactions.

### I. INTRODUCTION

The compound nucleus formed in a heavy-ion-induced fusion reaction usually has a large amount of excitation energy ( $E$ ) and angular momentum ( $I$ ). The emission of particles proceeds immediately and brings the nuclear excitation energy down to about one neutron binding energy above the yrast line. From there,  $\gamma$ -ray decay removes the rest of the excitation energy and angular momentum. The point at which  $\gamma$ -ray emission begins is called the "entry state" and it has a wide distribution both in angular momentum and excitation energy. The  $\gamma$  rays emitted in the early stages of the decay are from regions of high level density, and many decay pathways are possible. Therefore, these transitions appear as a continuum of  $\gamma$  rays. Eventually, all the decay pathways feed into yrast states and, subsequently, decay along the yrast line. These yrast transitions can be observed as discrete lines when enough intensity is accumulated.

The pathway of  $\gamma$  decay determines the correlation between the entry point and the feeding point. This pathway is mandated by the nuclear properties such as collectivity, moment of inertia, branching ratios, etc. Therefore, the variation of entry distribution with the spin of the yrast line may be used to study the nuclear properties in regions of high spin and temperature. Furthermore, this knowledge of entry point and cooling route is essential for the selection of the interesting decay pathways. Experimentally, this selection can be accomplished by gating on a particular region of ( $E, I$ ) space. For example, if large differences exist in entry distributions between the low spin and the high spin states, then it should be possible to enhance the population of high spin states for discrete line spectroscopy by appropriate ( $E, I$ ) gating.

The spin distribution of the entry state can be derived from  $\gamma$ -ray multiplicity measurements. Earlier experiments<sup>1,2</sup> have been able to characterize only the first and the second moments of the shape of the multiplicity distribution. Also, the distribution of excitation energy has

been measured<sup>3,4</sup> by using a  $\gamma$ -ray sum spectrometer. In general, it has been found that there is a fractionation of the angular momentum in (heavy ion, xn) reactions such that the channel emitting the least number of neutrons has the highest average angular momentum and excitation energy. Using the Spin Spectrometer, Sarantites *et al.*<sup>5</sup> measured the detailed shape of the entry-state distribution for each residual nucleus in several fusion reactions. In each case, the measured distributions agreed with the predictions of the statistical model. Additionally, studies<sup>6,7</sup> of the distribution of the entry states that feed specific yrast states of a given nucleus have also been carried out recently. In the present paper we report on our systematic study of several heavy-ion fusion reactions, done in the hope that we could obtain a more detailed understanding of the relation of the entry-state distribution and the population of the yrast states. A preliminary account of this work has been presented in Ref. 6.

### II. EXPERIMENTAL PROCEDURES AND DATA ANALYSIS

We have studied the nuclei produced in the reactions  $^{150}\text{Sm}(^{12}\text{C}, xn)^{158,159}\text{Er}$  with a 65-MeV  $^{12}\text{C}$  beam,  $^{100}\text{Mo}(^{34}\text{S}, 4n)^{130}\text{Ce}$  with a 144-MeV  $^{34}\text{S}$  beam, and  $^{70}\text{Zn}(^{50}\text{Ti}, xn)^{116,117}\text{Te}$  with a 170-MeV  $^{50}\text{Ti}$  beam. The beams were from the HHIRF tandem accelerator facility at the Oak Ridge National Laboratory. The  $\gamma$  rays from the compound nuclei were detected by using the Spin Spectrometer, a  $4\pi$  multielement  $\gamma$ -ray detector system which has been described in Ref. 8. Use of thin targets (about 1 mg/cm<sup>2</sup>) allowed the compound nucleus to recoil out of the target with almost uniform velocity and decay in flight. The Doppler shift was corrected for each detector by utilizing the known recoil velocity and the detector angle. In the experiment, two of the 70 NaI elements of the Spin Spectrometer were replaced by large volume (25% efficiency) high-resolution Ge detectors. data were recorded when there was a coincidence between either of

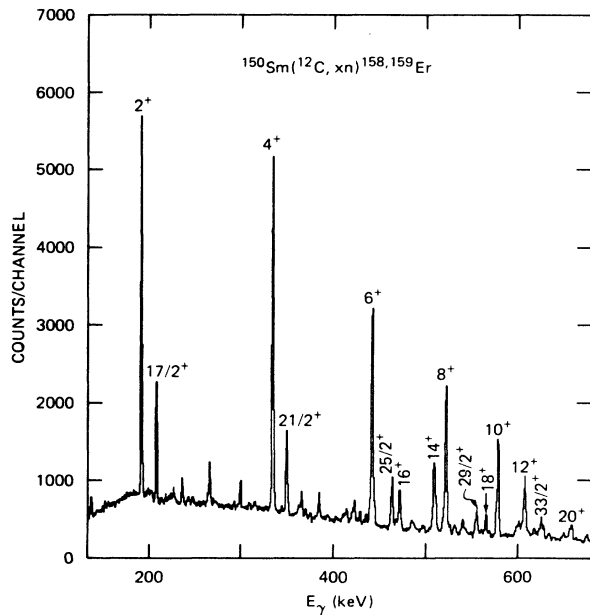


FIG. 1. The  $\gamma$ -ray spectrum obtained from the reaction  $^{150}\text{Sm}(^{12}\text{C}, xn)^{158,159}\text{Er}$  with a 65 MeV  $^{12}\text{C}$  beam. Yrast transitions from states of  $^{158}\text{Er}$  (integer spin) and from  $^{159}\text{Er}$  (half-integer spin) are shown.

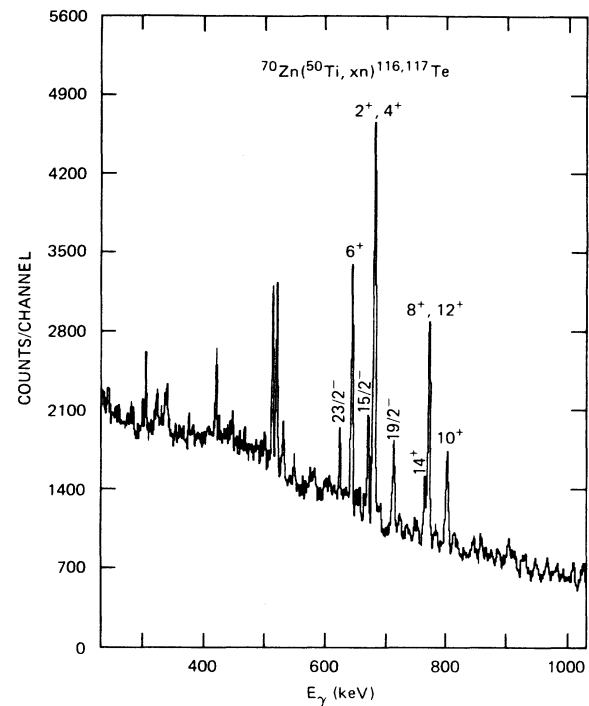


FIG. 3. The  $\gamma$ -ray spectrum obtained from the reaction  $^{70}\text{Zn}(^{50}\text{Ti}, xn)^{116,117}\text{Te}$  with a 170 MeV  $^{50}\text{Ti}$  beam. Yrast transition from states of  $^{116}\text{Te}$  (integer spin) and from  $^{117}\text{Te}$  (half-integer spin) are shown.

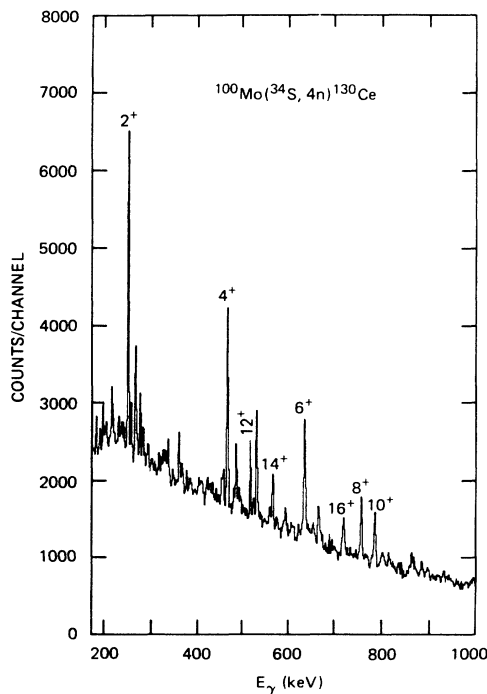


FIG. 2. The  $\gamma$ -ray spectrum obtained from the reaction  $^{100}\text{Mo}(^{34}\text{S}, 4n)^{130}\text{Ce}$  with a 144 MeV  $^{34}\text{S}$  beam. Transitions from yrast states are labeled with their spin values.

the Ge detectors and the Spin Spectrometer, with the additional requirement that four or more NaI detectors must fire. A total of about 30 million events were acquired for each of the experiment. Figures 1–3 show the Ge spectra from the three reactions employed here.

In the off-line analysis, the total pulse height ( $H$ ) and coincidence fold ( $k$ ) for each event were deduced from the pulse height of the individual NaI detectors after energy and time calibration and the removal of neutron pulses by time of flight. Next, the two-dimensional distribution of  $(H, k)$  was obtained by sorting events in coincidence with discrete transitions and by correcting this distribution for background under the gated peak with data from several background regions of the Ge spectra. Since these distributions do not include the gating  $\gamma$  ray observed in the Ge detectors, each distribution is shifted down in  $H$  by an amount proportional to the decay of this  $\gamma$  ray. In addition, not having this  $\gamma$  ray causes a reduction in  $k$  equal to its energy-dependent trigger efficiency. Since the gating  $\gamma$  rays have energies varying from 0.2 to 0.8 MeV, this exclusion creates appreciable distortion of the  $(H, k)$  distribution, especially when changes in the distribution are examined as a function of spin. To correct for the trigger bias effect it is necessary to include the missing  $\gamma$  ray in the  $(H, k)$  distribution. This was accomplished by first obtaining the  $(H, k)$  response function for the missing  $\gamma$  ray based on the calibration with  $\gamma$ -ray sources. Then, the total distribution was obtained by convoluting this single

$\gamma$ -ray distribution with the measured  $(H, k)$  distribution from the Spin Spectrometer. These corrected data give the distributions of entry states which feed the observed yrast states.

The entry distributions for the lowest excited states of the nuclei studied are shown in Figs. 4–6. In heavy-ion-induced fusion reactions, almost all the  $\gamma$ -ray decay goes through the lowest excited states. Thus, these distributions are assumed to represent the complete entry distribution of the corresponding reaction channels. It can be seen that these distributions are quite different in shape, but a common feature is the positive correlation between  $H$  and  $k$ . This correlation can be described by the two regression curves, defined as  $\bar{H}(k)$ , the mean values of  $H$  as a function of  $k$ , and  $\bar{k}(H)$ , the mean values of  $k$  as a function of  $H$ . These regression curves are also plotted in Figs. 4–6. The slopes of the two curves  $dk/d\bar{H}(k)$  and  $d\bar{k}(H)/dH$  at the peak of the distribution are listed in Table I. These two slopes are generally different, and only the former is likely to be parallel to the yrast line, because  $\bar{H}$  for a given  $k$  is about one neutron binding energy above the yrast line. Since the values of the two slopes are

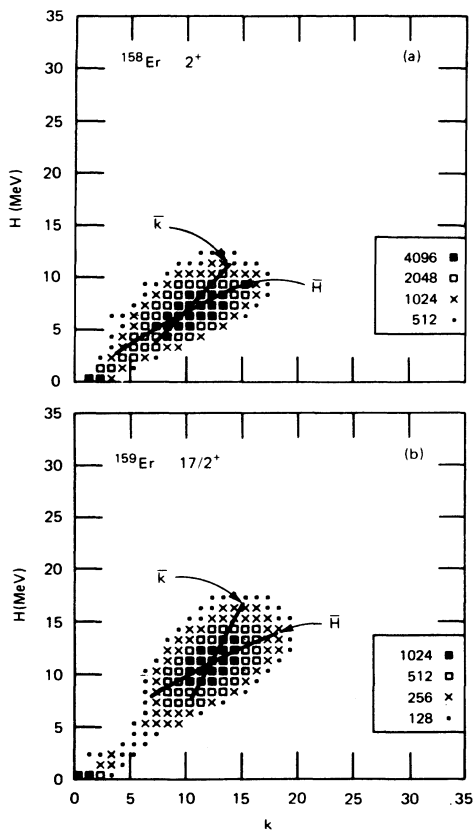


FIG. 4. Entry state distributions of total pulse height ( $H$ ) and coincidence fold ( $k$ ) obtained by gating (a) on the  $2^+ \rightarrow 0^+$  transition of  $^{158}\text{Er}$  and (b) on the  $\frac{17}{2}^+ \rightarrow \frac{13}{2}^+$  transition of  $^{159}\text{Er}$ . The regression curve  $\bar{H}$  is the average value of  $H$  for each  $k$ ; the curve  $\bar{k}$  is the average value of  $k$  for each  $H$ .

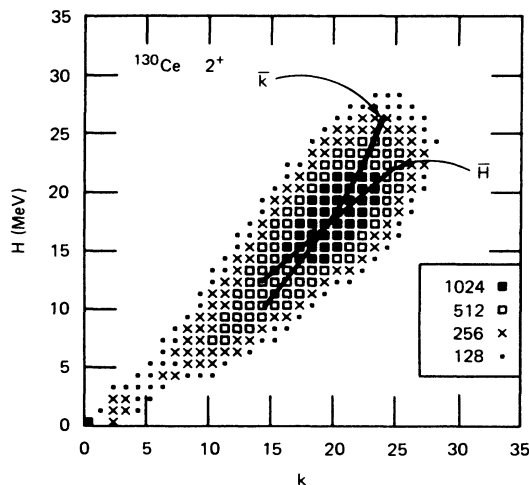


FIG. 5. Entry-state distribution obtained by gating on the  $2^+ \rightarrow 0^+$  transition of  $^{130}\text{Ce}$ . The two regression curves of the distribution are also shown.

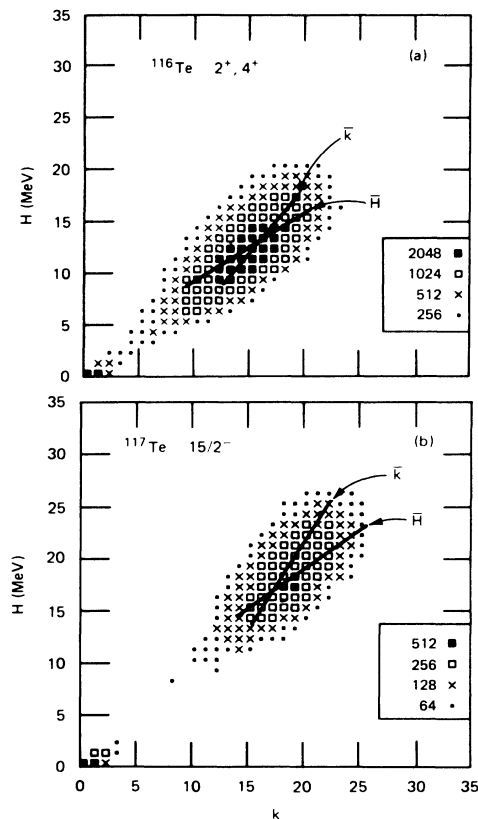


FIG. 6. Entry-state distributions obtained by gating (a) on the  $2^+ \rightarrow 0^+$  and  $4^+ \rightarrow 2^+$  of  $^{116}\text{Te}$  and (b)  $\frac{15}{2}^- \rightarrow \frac{11}{2}^-$  of  $^{117}\text{Te}$ . The two regression curves of the distribution are also shown.

TABLE I. Slope of the two regression curves of the entry-state distribution of the lowest yrast transition at the peak of the distribution (see Figs. 4–6).

	$I_i$	$I_f$	Slope ( $\text{MeV}^{-1}$ )	
			$dk/d\bar{H}(k)$	$d\bar{k}(H)/dH$
$^{158}\text{Er}$	2	0	1.84(0.31)	0.87(0.07)
$^{159}\text{Er}$	$\frac{17}{2}$	$\frac{13}{2}$	1.68(0.26)	0.62(0.06)
$^{130}\text{Ce}$	2	0	1.04(0.06)	0.68(0.03)
$^{116}\text{Te}$	2	0	1.47(0.20)	0.72(0.05)
$^{117}\text{Te}$	$\frac{15}{2}$	$\frac{11}{2}$	1.29(0.13)	0.56(0.04)

quite different, it is important to use the correct curve for the determination of the nuclear moment of inertia.

The important features of the  $(H, k)$  distribution are the position of the centroid and the width. These parameters can be extracted from the distribution by using the various moments of the distribution defined as

$$M'_{ij} = \int \rho(H, k) H^i k^j dH dk, \quad (1)$$

where  $\rho(H, k)$  is the normalized entry state distribution and is given by

$$\int \rho(H, k) dH dk = 1. \quad (2)$$

The two first moments are the mean values of  $H$  and  $k$ , respectively, i.e.,  $M'_{01} = \langle k \rangle$  and  $M'_{10} = \langle H \rangle$ . The values of the first moment for the yrast states measured in the present work are shown by the points in Figs. 7–9 for  $^{158,159}\text{Er}$ ,  $^{130}\text{Ce}$ , and  $^{116,117}\text{Te}$ , respectively. These values are obtained by averaging the results from the two gating Ge detectors. Inelastic excitation of the target nuclei and decay of the radioactive residual nuclei produce low multiplicity background events. Since the subtraction of background leaves large fluctuations in the low- $k$  region, this region was excluded from the moment calculation.

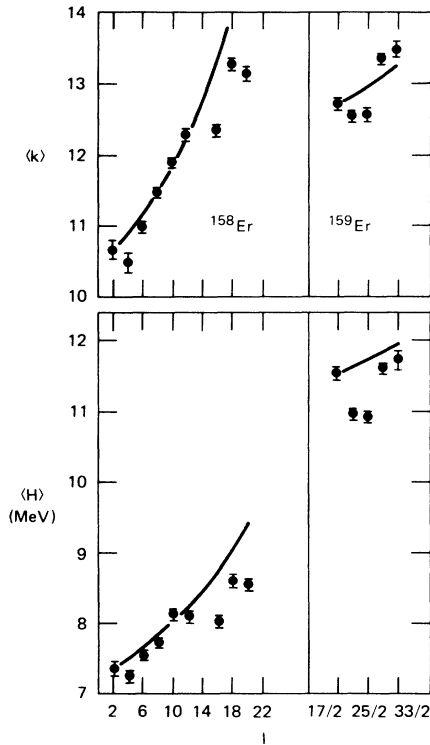


FIG. 7. The average values of  $k$  and  $H$  (the first moments of the entry distribution) for  $^{158}\text{Er}$  and  $^{159}\text{Er}$  as a function of the initial spin of the yrast transition are shown as points. The solid lines represent results of a model calculation described in the text.

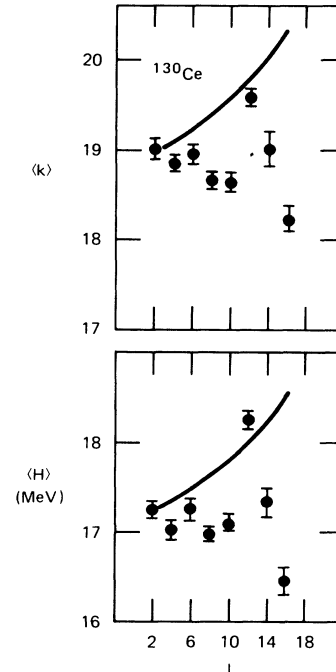


FIG. 8. The average values of  $k$  and  $H$  (the first moments of the entry distribution) for  $^{130}\text{Ce}$  as a function of the initial spin of the yrast transition.

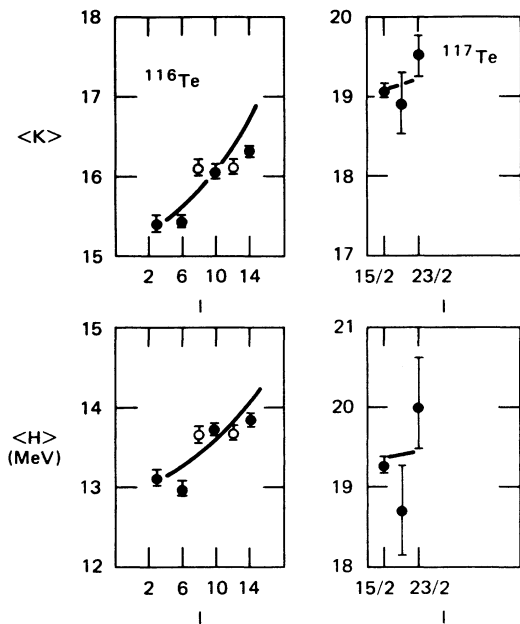


FIG. 9. The average values of  $k$  and  $H$  (the first moments of the entry distribution) for  $^{116}\text{Te}$  and  $^{117}\text{Te}$  as a function of the initial spin of the yrast transition.

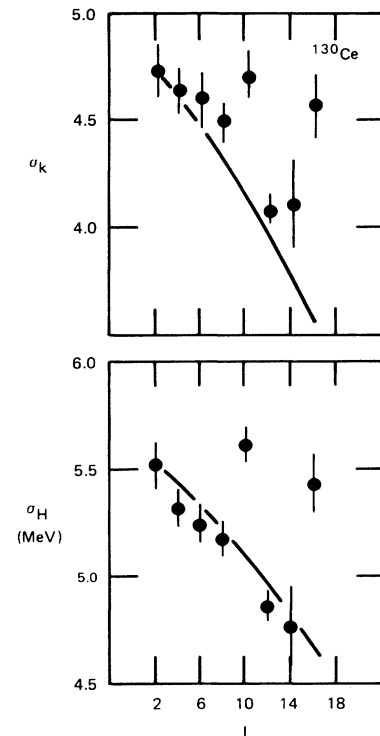


FIG. 11. The width of the entry state distribution (second moment) in  $k$  and  $H$  for  $^{130}\text{Ce}$  as a function of the spin of the yrast transition.

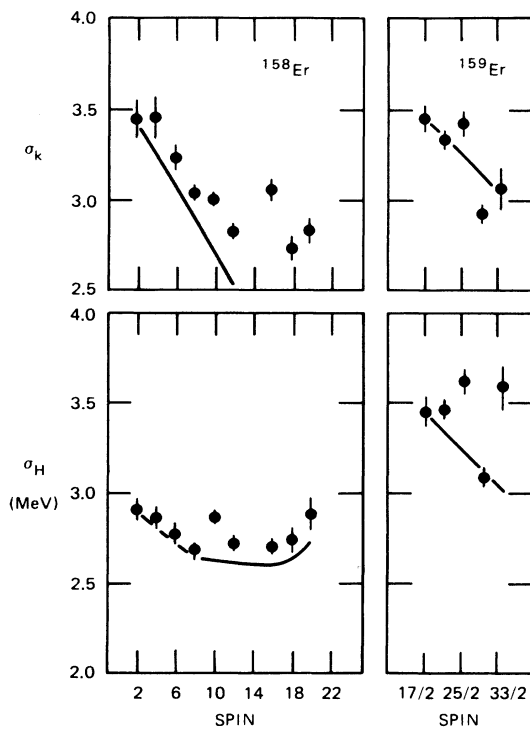


FIG. 10. The width of the entry state distribution (second moment) in  $k$  and  $H$  for  $^{158}\text{Er}$  and  $^{159}\text{Er}$  as a function of the spin of the yrast transition.

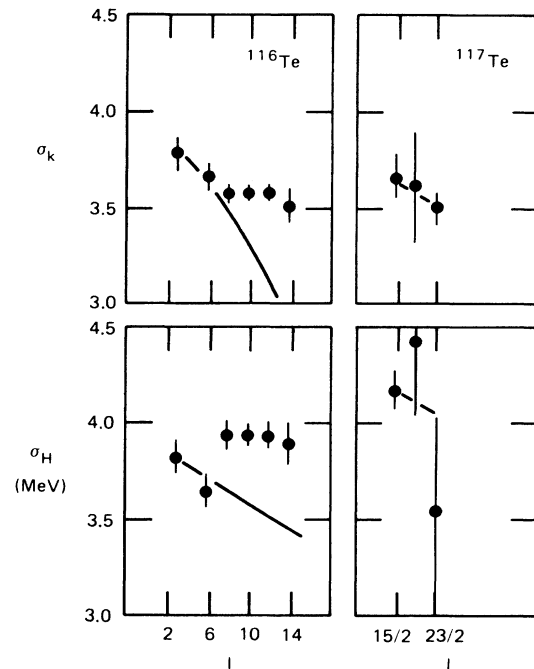


FIG. 12. The width of the entry state distribution (second moment) in  $k$  and  $H$  for  $^{116}\text{Te}$  and  $^{117}\text{Te}$  as a function of the spin of the yrast transition.

The low- $k$  cutoff value is four for the Er data and six for the Ce and Te data. The cutoff has very little effect on the results, since there are very few counts below these  $k$  values.

For higher moments it is more convenient to use the moments about the mean:

$$M_{ij} = \int \rho(H,k)(H - \langle H \rangle)^i (k - \langle k \rangle)^j dK dk. \quad (3)$$

The first moments about the mean are equal to zero by definition. The second moments  $M_{20}$  and  $M_{02}$  are the mean-square widths  $\sigma_H^2$  and  $\sigma_k^2$  of the distribution projected on the  $H$  and  $k$  axes, and  $M_{11}$  is a measure of the correlation between  $H$  and  $k$ . The root-mean-square widths  $\sigma_H, \sigma_k$  are shown in Figs. 10–12. A different way to represent the second moments is to rotate the axes around  $H = \langle H \rangle$  and  $k = \langle k \rangle$  by angle  $\theta$ , to set  $M_{11} = 0$

TABLE II. Values of the width of the entry state distribution in the principle coordinates, and the angle of the principle axis.

$I$	$\sigma_u$	$\sigma_v$	$\theta$
$^{158}\text{Er}$			
2	4.09(0.13)	1.90(0.01)	37.6(0.3)
4	4.11(0.14)	1.84(0.02)	37.1(0.2)
6	3.86(0.08)	1.83(0.01)	38.0(0.2)
8	3.66(0.05)	1.77(0.02)	39.3(0.3)
10	3.74(0.05)	1.81(0.01)	42.7(0.2)
12	3.53(0.04)	1.71(0.02)	43.3(0.2)
16	3.72(0.07)	1.70(0.03)	39.5(0.8)
18	3.49(0.09)	1.69(0.04)	45.1(1.5)
20	3.70(0.09)	1.68(0.06)	45.5(0.5)
$^{159}\text{Er}$			
$\frac{17}{2}$	4.39(0.11)	2.19(0.04)	44.8(0.2)
$\frac{21}{2}$	4.30(0.06)	2.16(0.02)	46.7(0.2)
$\frac{25}{2}$	4.54(0.09)	2.09(0.02)	47.3(0.2)
$\frac{29}{2}$	3.74(0.08)	2.04(0.04)	47.8(0.5)
$\frac{33}{2}$	4.25(0.19)	2.05(0.03)	52.2(0.4)
$^{130}\text{Ce}$			
2	6.86(0.16)	2.43(0.02)	50.7(0.4)
4	6.67(0.14)	2.36(0.02)	50.1(0.3)
6	6.58(0.15)	2.37(0.02)	49.8(0.3)
8	6.48(0.13)	2.26(0.04)	50.2(0.2)
10	6.97(0.12)	2.27(0.04)	51.3(0.3)
12	5.90(0.08)	2.36(0.05)	52.1(0.2)
14	5.88(0.29)	2.27(0.05)	50.8(0.5)
16	6.74(0.18)	2.26(0.06)	51.1(0.4)
$^{116}\text{Te}$			
2,4	4.86(0.12)	2.20(0.03)	45.55(0.40)
6	4.71(0.10)	2.14(0.03)	44.84(0.24)
8,12	4.87(0.07)	2.16(0.03)	49.07(0.15)
10	4.87(0.04)	2.16(0.02)	49.11(0.18)
14	4.80(0.10)	2.13(0.02)	49.56(0.20)
$^{117}\text{Te}$			
$\frac{15}{2}$	5.08(0.14)	2.25(0.02)	50.83(0.40)
$\frac{19}{2}$	5.24(0.50)	2.28(0.02)	53.62(0.50)
$\frac{23}{2}$	4.50(0.40)	2.14(0.09)	44.89(5.4)

TABLE III. Comparison of moments of experimental and calculated entry state distributions (see the text of definitions of variables).

	<sup>158</sup> Er		<sup>159</sup> Er		<sup>130</sup> Ce	
	Expt.	Calc.	Expt.	Calc.	Expt.	Calc.
$\langle k \rangle$	10.6	9.9	12.7	14.3	19.0	19.4
$\sigma_k$	3.5	2.9	3.5	3.5	4.7	3.7
$\langle H \rangle$	7.4	7.4	11.6	12.5	17.3	19.3
$\sigma_H$	2.9	1.9	3.5	2.5	5.5	3.3
$\sigma_u$	4.1	3.2	4.4	4.1	6.9	4.7
$\sigma_v$	1.9	1.3	2.2	1.5	2.4	1.8
$\theta$	38	28	45	32	51	41

in the new coordinate system. The axes of the new coordinate system ( $u, v$ ) are the principal axes of the second moment. It can be shown that

$$\tan 2\theta = \frac{2M_{11}}{M_{02} - M_{20}} \quad (4)$$

In the ( $u, v$ ) system, the width of the distribution can be characterized by the diagonalized width  $\sigma_u$  and  $\sigma_v$ . The diagonalized width  $\sigma_u, \sigma_v$  and the angle  $\theta$  between the  $k$  and  $u$  axes are listed in Table II.

### III. DISCUSSION

The entry state distributions for the evaporation residues can be calculated from the statistical model. Calculations were made using the program PACE2 (Ref. 9) for <sup>130</sup>Ce and <sup>158,159</sup>Er. The calculations were done with a level density parameter  $a = A/8.5$ , an electric dipole gam-

ma ray strength function reflecting the systematics of the giant dipole resonance, and an initial spin distribution obtained from the Bass potential.<sup>10</sup> The ( $E, M$ ) distributions from these calculations were then convoluted with the response of the Spin Spectrometer to generate ( $H, k$ ) distributions. Table III compares the moments of these ( $H, k$ ) distributions with the moments of the experimental distributions. The first moments  $\langle k \rangle$  and  $\langle H \rangle$  are well reproduced by the calculation, but the experimental widths are in general 20–30% larger than the calculation. While no attempt was made to vary parameters of the calculation to improve the agreement with data, the failure to account for widths, other than  $\sigma_k$ , is a chronic deficiency<sup>11</sup> of statistical calculations which do not include details of nuclear structure, such as distribution of collective  $E2$  gamma strength well above the yrast line. A principal motivation for including this comparison is to illustrate the value of moments with respect to the principle axes of the ( $E, M$ ) distributions in providing a concise description of the distributions.

The variation of the entry distribution as a function of the spin of the yrast transition is the primary point of interest in the present work. As can be seen in Figs. 7–9, the values of  $\langle k \rangle$  and  $\langle H \rangle$  increase at high spin as expected from the simple picture that high-spin yrast states are fed mainly from the high-spin and high-excitation energy region of the entry state. The above picture can be better understood in terms of a simple model which assumes that a yrast state with spin  $I$  is fed from the entire entry region of this reaction channel with spin  $\geq I$  and that the nucleus decays mainly through stretched  $E2$  transitions. Thus, it allows us to calculate the expected  $\langle k \rangle$  and  $\langle H \rangle$  values for any state from the measured ( $H, k$ ) distribution of the lowest excited state by using a higher value of  $k$  cutoff according to

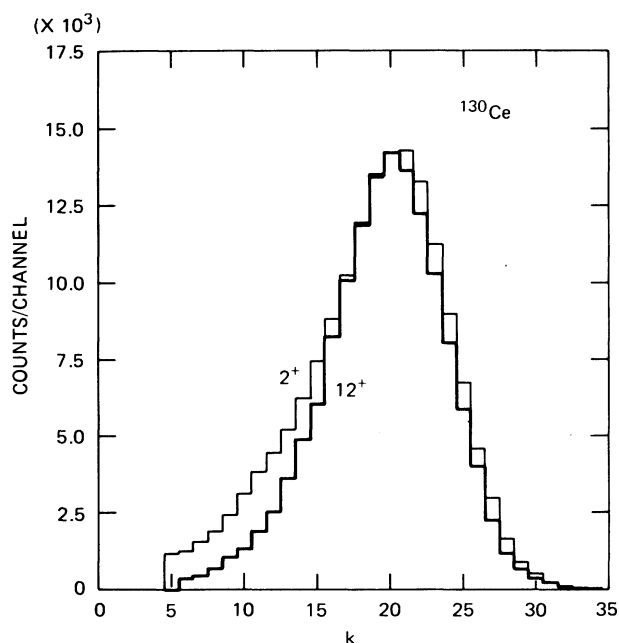


FIG. 13. The  $k$  projection of the entry distribution of the  $2^+$  and  $12^+$  states of <sup>130</sup>Ce.

TABLE IV. Channel resolution of  $H$  and  $k$  distributions.

	$\Delta H / \sigma_H(R)$	$\Delta k / \sigma_k(R)$
<sup>158</sup> Er	1.91	0.53
<sup>159</sup> Er	1.48	0.54
<sup>116</sup> Te	1.70	1.13
<sup>117</sup> Te	1.55	1.24

TABLE V. Sensitivity in selectively populating high spin states.

	$\frac{d\langle H \rangle}{dI/2} \frac{1}{\sigma_H}$	$\frac{d\langle k \rangle}{dI/2} \frac{1}{\sigma_k}$
$^{158}\text{Er}$	0.052	0.089
$^{130}\text{Ce}$	0.0	0.0
$^{116}\text{Te}$	0.037	0.050

$$k_{\min}(I) = k_{\min}(I_1) + (I - I_1)/2. \quad (5)$$

where  $I_1$  is the spin of the first excited state and  $k_{\min}(I_1)$  is the  $k$  cutoff value discussed before. This procedure is justified for the Spin Spectrometer data because the value of the fold  $k$  is quite close to the  $\gamma$ -ray multiplicity  $M$  for  $10 < k < 20$ . (See Ref. 8.) Results of the model predictions, which provide only an upper limit, are shown as solid lines in Figs. 7–9. Several interesting features are obvious in these figures. First, for  $^{130}\text{Ce}$  the  $\langle k \rangle$  and  $\langle H \rangle$  values do not increase with spin as predicted by the model. This effect may be due to the high degree of mixing of the decay pathways in the high-spin and high-excitation-energy region. Such mixing could wash out the spin correspondence between the entry state and the yrast state. However, the data from  $^{158}\text{Er}$  and  $^{116}\text{Te}$  more nearly follow the general behavior of the model predictions. This may indicate that the nuclear properties of  $^{130}\text{Ce}$  in the entry region are different from  $^{158}\text{Er}$  and  $^{116}\text{Te}$ . A second effect is observed in  $^{130}\text{Ce}$  which exhibits an increase in the  $\langle H \rangle$  and  $\langle k \rangle$  values at the spin 12 state immediately above the backbending. Figure 13 shows the  $k$  projection of the entry distribution of the  $2^+$  state and  $12^+$  state of  $^{130}\text{Ce}$ . It is clear from the comparison that the  $12^+$  distribution has a reduction in the low- $k$  component. Detailed discrete line  $\gamma$ -ray spectroscopy results<sup>12</sup> do not show discrete line side feeding into the  $12^+$  state. This may be due to the fact that the ground-state band and bands with similar moments of inertia extend into the high-spin and high-excitation-energy region. These bands have steeper slopes than the yrast line and therefore they channel their decay from above the backbending region through pathways leading into region below the backbend. The states just above the backbending will be fed mostly from the higher spin region. As seen in Figs. 7 and 9, this effect is not observed in Er or Te. On the contrary, they follow the prediction of the simple model rather closely, except for the high spin states in  $^{158}\text{Er}$ . These high spin points lie below the model predictions, probably as a result of having reached the maximum values of angular momentum of the reaction.

The measured widths of the  $(H, k)$  distributions for the nuclei studied here are plotted in Figs. 10–12. In general, the width becomes smaller for the higher spin states. This indicates that the higher-spin states are fed from a narrower entry region. The simple calculations reproduce the general behavior rather well. The reduction of the width for a given spin is smaller for the reaction channel with

higher  $\langle H \rangle$  and  $\langle k \rangle$  values. This has most likely the same cause as the low sensitivity of the  $\langle H \rangle$  and  $\langle k \rangle$  values. On the other hand, for  $^{158}\text{Er}$ , due to a larger spread in  $H$  in the high- $k$  region, the width  $\sigma_H$  increases for high spin states. This is also in agreement with the predictions of the simple model discussed above.

In certain spectroscopy experiments the values of  $H$  and  $k$  are used as a selection parameter to separate different reaction channels. In such an application, the ability to enhance a given reaction channel depends on the separation of the centroids of the distributions ( $\Delta H$  and  $\Delta k$ ) and the width of the channel to be rejected [ $\sigma_H(R), \sigma_k(R)$ ]. The ratio of these numbers, i.e.,  $\Delta H/\sigma_H(R)$  and  $\Delta k/\sigma_k(R)$ , are the important parameters. The larger these ratios, the easier it becomes to enhance the desired reaction channel. The values for  $^{158,159}\text{Er}$  and  $^{116,117}\text{Te}$  are shown in Table IV. It is obvious for the cases shown here that the total pulse height  $H$  is a more effective parameter for separating reaction channels. This may be because  $H$  is proportional to  $I^2$ , while  $k$  is proportional to  $I$ .

If one is to utilize the  $(H, k)$  gating for selecting high-spin yrast states of a given nucleus, it is necessary to have a significant difference in the  $(H, k)$  distribution for high- and low-spin states. The sensitivity of this method depends on the change of the  $\langle H \rangle$  and  $\langle k \rangle$  values as a function of spin. This sensitivity can be defined as

$$\frac{d\langle H \rangle}{dI/2} \frac{1}{\sigma_H} \quad \text{and} \quad \frac{d\langle k \rangle}{dI/2} \frac{1}{\sigma_k}.$$

In Table V, we have shown these ratios for  $^{158,159}\text{Er}$ ,  $^{130}\text{Ce}$ , and  $^{116,117}\text{Te}$  obtained by averaging over all the transitions. As can be seen, the sensitivities are very small, indicating this method is not very effective in selecting high spin states.

In conclusion, the measured shapes of the entry-state distribution from the present experiment change slowly with the spin of the gating yrast transition. It appears that in the formation of a compound nucleus, the channel formed with higher angular momentum has lower sensitivity of entry state population on the spin of the yrast transition. This is mainly due to the lack of direct feeding and the mixing of the nuclear decay pathways between the entry region and the yrast line. With the low sensitivity observed in the present experiments, it would be very ineffective to attempt to use  $H$  and  $k$  selection to enhance the population of high-spin states in these nuclei. On the other hand, the separation of reaction channel can be achieved efficiently. Whether these features are true in general has to be determined from the study of many more reaction systems.

#### ACKNOWLEDGMENTS

This research was supported by the U.S. Department of Energy under Contract No. DE-AC05-84OR21400 with Martin Marietta Energy Systems, Inc. Research at Washington University was supported by the U.S. Department of Energy under Contract No. DE-AS02-76ER04052.

- \*Permanent address: The Australian National University, Canberra, Australian Capital Territories 2600, Australia.
- <sup>1</sup>G. B. Hagemann, R. Broda, B. Herskind, M. Ishihara, S. Ogaza, and H. Ryde, *Nucl. Phys.* **A245**, 166 (1975).
- <sup>2</sup>D. G. Sarantites, J. H. Barker, M. L. Halbert, D. C. Hensley, R. A. Dayras, E. Eichler, N. R. Johnson, and S. A. Gronemeyer, *Phys. Rev. C* **14**, 2138 (1975).
- <sup>3</sup>P. O. Tjøm, I. Espe, G. B. Hageman, B. Herskind, and D. L. Hillis, *Phys. Lett.* **72B**, 439 (1978).
- <sup>4</sup>F. Folkmann, J. D. Garrett, G. D. Hagemann, M. N. Harakeh, B. Herskind, D. L. Hillis, S. Ogaza, H. Emling, E. Grosse, and D. Schwalm, *Nucl. Phys.* **A361**, 242 (1981).
- <sup>5</sup>D. G. Sarantites *et al.*, *Phys. Lett.* **115B**, 441 (1982).
- <sup>6</sup>I. Y. Lee, C. Baktash, J. R. Beene, M. P. Fewell, M. L. Halbert, N. R. Johnson, F. K. McGowan, W. T. Milner, H. Kim, D. G. Sarantites, and R. O. Sayer, Oak Ridge National Laboratory Physics Division Progress Report, 1983, Oak Ridge National Laboratory Report ORNL-6004, 1983, p. 108.
- <sup>7</sup>A. J. Larabee, L. L. Riedinger, C. R. Bingham, L. H. Courtney, C. Baktash, M. L. Halbert, D. C. Hensley, N. R. Johnson, I. Y. Lee, Y. Schutz, S. A. Hjorth, A. Johnson, K. J. Nyberg, B. Herskind, A. Dilmanian, M. Rajagopalan, D. G. Sarantites, D. R. Haenni, J. C. Waddington, J. S. Hattula, and G. A. Leander, *Bull. Am. Phys. Soc.* **30**, 761 (1985).
- <sup>8</sup>M. Jääskeläinen, D. C. Hensley, M. L. Halbert, J. H. Barker, R. Jääskeläinen, D. G. Sarantites, R. Woodward, F. A. Dilmanian, and J. T. Hood, *Nucl. Instrum. Methods* **204**, 385 (1983).
- <sup>9</sup>A. Gavron, *Phys. Rev. C* **21**, 238 (1980).
- <sup>10</sup>R. Bass, *Phys. Rev. Lett.* **39**, 265 (1977).
- <sup>11</sup>D. G. Sarantites, M. Jääskeläinen, R. Woodward, F. A. Dilmanian, D. C. Hensley, J. H. Barker, J. R. Beene, M. L. Halbert, and W. T. Milner, *Phys. Lett.* **115B**, 441 (1982).
- <sup>12</sup>P. J. Nolan, D. M. Todd, P. J. Smith, D. J. G. Love, P. J. Twin, O. Andersen, J. D. Garrett, G. B. Hagemann, and B. Herskind, *Phys. Lett.* **108B**, 269 (1982).